Eur. Phys. J. B **26**, 297–300 (2002)
DOI: 10.1140/epjb/e20020092

THE EUROPEAN PHYSICAL JOURNAL B
EDP Sciences

MO analysis of macroscopic supercurrent flow in MgB_2

R. Gerbaldo[1], G. Ghigo[1], G. Giunchi[2], L. Gozzelino[1], F. Laviano[1], and E. Mezzetti[1,a]

[1] INFM - U.d.R Torino-Politecnico; INFN - Sez. Torino; Politecnico di Torino, c.so Duca degli Abruzzi 24, 10129 Torino, Italy
[2] Edison S.p.A, Foro Buonaparte 31, 20121 Milano, Italy

Received 31 May 2001 and Received in final form 5 December 2001

Abstract. We present results from an extended magneto-optical (MO) analysis of two samples cut from high-density pellets of MgB_2. The first sample was studied in order to show that no matter how large the sample is and despite the bulk granularity, the material enters into a critical state in a crystal-like fashion. The second sample was chosen for the quantitative analysis. A numerical approach based on an inverted 2D Biot-Savart model was used to calculate the current paths across the homogeneous polycrystalline bulk, as well as in the vicinity and across some morphological defects. Local current densities in the homogeneous part were estimated as a function of the applied magnetic field at different temperatures, in three regimes: below full penetration, at full penetration and above full penetration, respectively. A hypothesis of interpretation of the apparent absence of magnetic granularity inside the polycrystalline microstructure is presented. It is related to a critical state likely reached by a network of strongly coupled Josephson junctions.

PACS. 74.70.-b Superconducting materials (excluding high-T_c compounds) – 74.50.+r Proximity effects, weak links, tunneling phenomena, and Josephson effects – 74.80.-g Spatially inhomogeneous structures

Introduction

In this paper we report on a quantitative magneto-optical (MO) analysis of bulk MgB_2. The MO technique [1] offers a powerful tool to investigate the correlation between microstructure and magnetic granularity in such new compound [2–7]. We studied, with a quantitative approach, the magnetic field distributions and the macroscopic supercurrent flow across samples cut from high quality pellets of MgB_2. The micro-structural investigation exhibits features typical of polycrystalline material. Large grains of about ten microns in diameter are framed inside a matrix of micro-crystals, whose size is one order of magnitude lower than the grains. In this paper we report strong evidences of the fact that the material enters into a critical state in a crystal-like fashion. The further evidence of an intergranular current density is a forthcoming issue. The magnitude and direction of this current is calculated in different regimes, below and above the full penetration field. In all these regimes the signature of strong pinning is shown and preliminarily discussed.

Experimental details

High density MgB_2 bulk pellets were prepared starting from the elemental compounds B (99.5% of purity) and Mg (99.9% of purity), after their reaction in a sealed stainless steel container, lined with a Nb foil. The thermal treatment was performed for two hours in the range of 850 °C–950 °C. The preparation procedures of highly densified MgB_2 pellets are reported elsewhere [8]. The MO analysis is performed inside a modified commercial cryostat whose temperature is controlled from 4 to 300 K [9]. For the present investigation two samples were cut from a polycrystalline pellet. The sample #1 has irregular parallelepiped shape and measures (≈12.0 mm × 8.1 mm × 0.96 mm). Although it is too large to allow a quantitative MO analysis with our equipment, it was selected to show how the general aspects related to the flux penetration do not depend on the sample dimension. Sample #2 size is (4.7 mm × 2.0 mm × 1.9 mm) and its shape is a quasi-regular parallelepiped. This specimen was chosen for the extended analysis to show the flux-penetration i) into a continuous-bulk granular structure, ii) inside a macroscopic crack and iii) inside a zone where the streamline is perturbed by a channeling of the flux into a "bottle neck" [10].

Experimental results

Here we report on two kinds of measurements:

i) zero field cooling, ZFC (starting from a temperature above the transition, the sample is cooled down to 4 K

[a] e-mail: mezzetti@polito.it

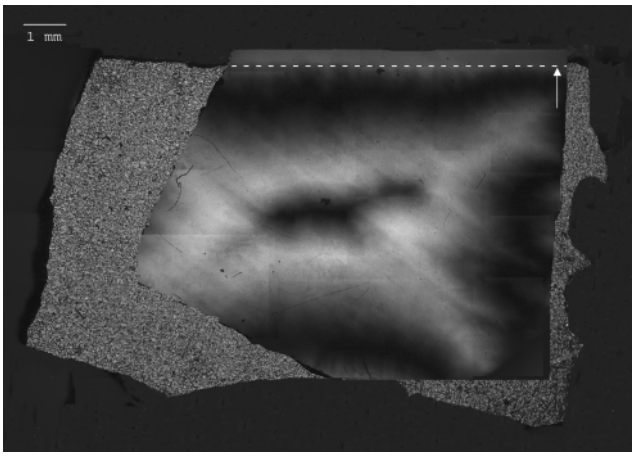

Fig. 1. Sample #1. MO image in remnant state at 35 K and after the application of an external field $\mu_0 H = 180$ mT. An edge of the sample is visible in the upper part (arrow); two edges of the indicator film are visible on the left. In the centre there is a totally screened region showing the main characteristics of a critical state. Minor deviations from an ideal critical state penetration are due to the irregular shape of the sample. In the background the optical image of the sample is shown in order to put in evidence the sample edges.

under zero magnetic field, then warmed up and measured at different temperatures and fields);

ii) remnant state, RS (the sample is cooled down to the working temperature, under zero magnetic field, after that a given field is applied and removed while the image is taken as soon as the field is removed).

Figure 1 represents the MO picture of the sample #1 at 35 K in the remnant state, after the switching off of an external magnetic field of 180 mT (sweeping time to zero field and acquisition time ∼1 s). As mentioned before, the sample size is too large to observe the entire geometry, therefore it was necessary to merge several pictures. Due to the fact that a wider scale image is not possible without displacement of the iron garnet during the experiment (that would invalidate the result) and because we already used the maximum visual field available, we add the optical image of the sample in the background in order to underline the sample edges. The observed MO pattern evolves as follows: with the external field applied, the magnetic flux penetrates the sample mainly from the central part of the borders and it is pushed away from the bisectors of the corners. When the applied field is removed, the current flowing along the edges changes direction and the flux is driven towards the corners. The pixels of maximum light intensity in the picture represent the position reached by the flux front in the steady state before the field removal. The convex shape of the flux front is labelled by discontinuity lines [11–16], referred to in more detail along the text. All these features are characteristic of a "crystal" near the critical state regime. The outstanding consequence is that, in spite of its granular nature, the sample enters into a critical state in a crystal-like fashion.

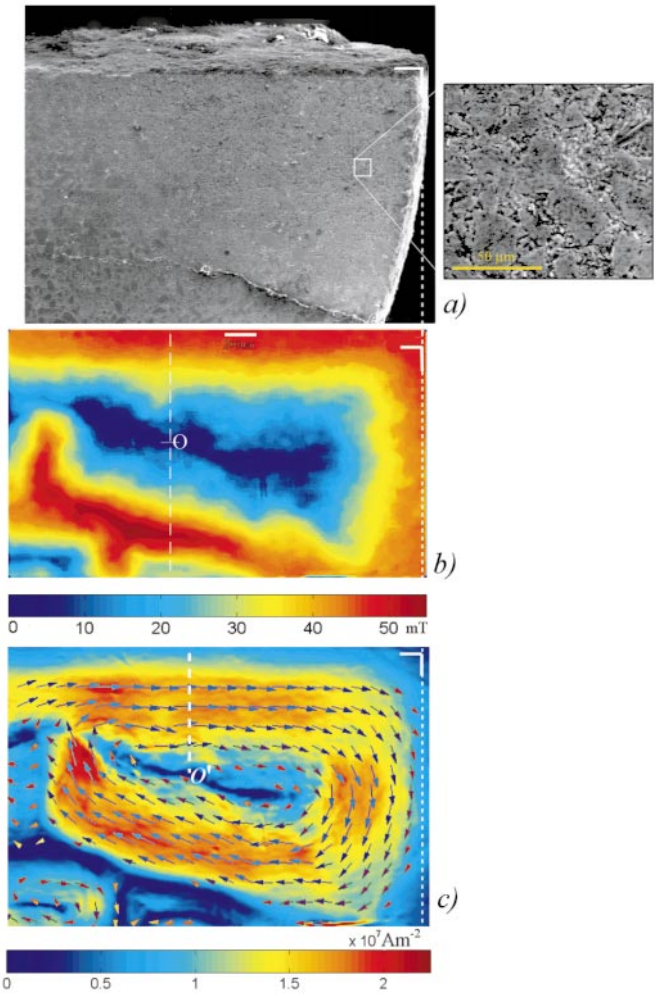

Fig. 2. Sample #2. The figures are aligned along the dotted line; the spatial scale bar is unique and placed in Figure 2b. (a) SEM image. The inset shows a magnification of the framed part of the figure. (b) Magnetic induction map taken in zero field cooling regime at $T = 35$ K and $\mu_0 H = 51$ mT. The bottom bar indicates the field scale. For comparison between pattern shapes see reference [10]. (c) Vector plot (arrows) and current magnitude map (colors) as drawn from the inversion of the induction data of Figure 2b at $T = 35$ K and $\mu_0 H = 51$ mT.

In an early work [3] this feature was not directly observed, while it was observed in reference [4].

Henceforth a more extended analysis of sample #2 is discussed. The granular microstructure and a macroscopic crack are clearly visible in the SEM (Scanning Electron Microscopy) image (Fig. 2a). The crack is characterized by a zone of "correlated holes" terminating in the central part with some vanishing pattern that cannot be seen by the optical analysis and can be scarcely seen by the SEM analysis. This "hidden" pattern can be very clearly identified by means of the MO analysis as a source of magnetic granularity.

Figure 2b shows a field map obtained from a MO image by means of a careful non-linear calibration [9]. Inside the trapezoidal shaped insula, the typical horn-shaped pattern, which corresponds to the discontinuity lines observed

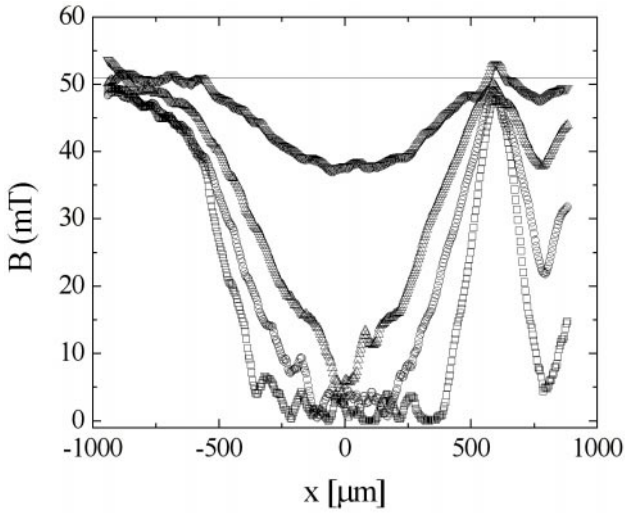

Fig. 3. Sample #2. Magnetic induction profiles evaluated in correspondence of the white dashed line of Figure 2b at 30 (-□-), 34 (-○-), 35 (-△-), 36 (-∇-) K, respectively. The origin of the x-axis is shown in Figure 2b.

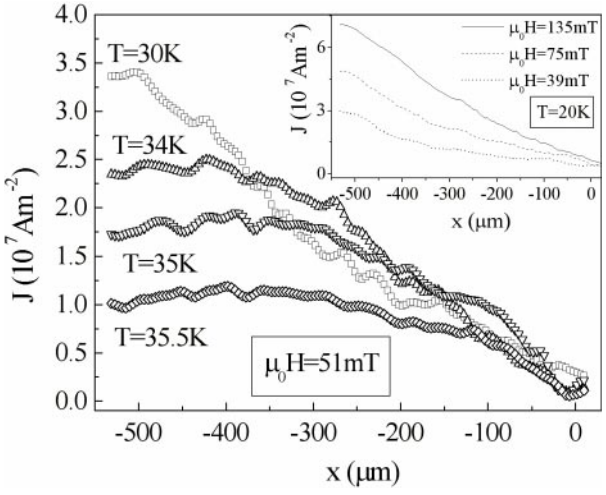

Fig. 4. Sample #2. Local current profiles evaluated in correspondence of the white dashed line of Figure 2c at different temperatures and $\mu_0 H = 51$ mT. The origin of the x-axis is shown in Figure 2c. Inset: local current profiles evaluated at $T = 20$ K and different applied magnetic fields.

by Schuster *et al.* [14,15] (d+ lines) and attributed to the current path bending, is visible. According to the calculation of reference [16] these patterns are due to a critical state of nearly constant J_c inside the sample. The measure is performed at 35 K with an external field of 51 mT after ZFC. Figure 3 shows flux profiles along the dashed line drawn in Figure 2b, evaluated at the same applied field of 51 mT at different temperatures. The observable fields by MO analysis are large enough to cause a critical state (*i.e.* full penetration of the magnetic flux) only above 34 K. The position of the profile tracking line is chosen in this case to point out the slightly higher slope near the banks of the crack. The higher slope is due to the shielding currents at the boundary with the not superconducting crack region (dark red spot near the bottom).

Starting from the measured value of magnetic induction $\mathbf{B}(\mathbf{r})$ and from the applied field $\mathbf{H}_a$, we can reconstruct both the modulus and the direction of the current density inside the sample, $\mathbf{J}(\mathbf{r})$, through the inversion of the Biot-Savart law:

$$\mathbf{B}(\mathbf{r}) - \mu_0 \mathbf{H}_a = \frac{\mu_0}{4\pi} \int d\mathbf{r}' \frac{\mathbf{J}(\mathbf{r}') \wedge (\mathbf{r} - \mathbf{r}')}{|\mathbf{r} - \mathbf{r}'|}.$$

Following references [17,18], the convolution theorem is used to transform the involved fields into the Fourier space. The numerical method, containing a Fast Fourier Transform-based algorithm, allows to calculate modulus and direction of the electrical current density distribution in the plane of the MO indicator, averaged over the sample thickness. Our method will be described in detail in a forthcoming paper.

Figure 2c shows the local current intensity map as a background picture for the current-path map. The streamline loops around the trapezoidal island are the main features. In the left part of the crystal, the constriction creates a superconducting bridge where the flux gradient as well as the supercurrent stationary flow ($\nabla \cdot \mathbf{J} = 0$) is modified, as emphasized in the vector plot of the current streamlines. The current bending is determined by the boundary conditions across two regions of different critical currents.

In Figure 4 current profiles along the white dashed line in Figure 2c are plotted at different temperatures and $\mu_0 H = 51$ mT. The flux, penetrating from outside, determines the pinning-dominated band with $J \approx J_c$. On the contrary, the central region is not penetrated by the flux, and the shielding current, as expected for confined transverse geometries, crosses it [19]. The size of this region varies because, as the temperature increases, the flux front proceeds towards the center of the sample. The inset of Figure 4 shows the local current profiles at $T = 20$ K. At this temperature the flux is not penetrated inside the sample, so we observe only the shielding contribute to the current. This is demonstrated by the positive curvature of the profile, and by the increasing of the current maximum value with the external field. As the temperature increases, the current density starts to saturate to J_c (at different fields) and full penetration of flux and critical current gradually sets up (critical state) [20].

The quantitative results concerning the white dashed line of Figure 2c are summarised in Figure 5. Namely, the local current density values along this line can be considered as representative of the sample state in different phase points. The maximum values of the current along profile as those in Figure 4 are plotted as a function of the applied field and temperature. The evaluated currents are the macroscopic currents (shielding + pinning contributes) in different phase points of the specimen. Three maximum current density regimes, below full penetration, at full penetration and above full penetration, are once

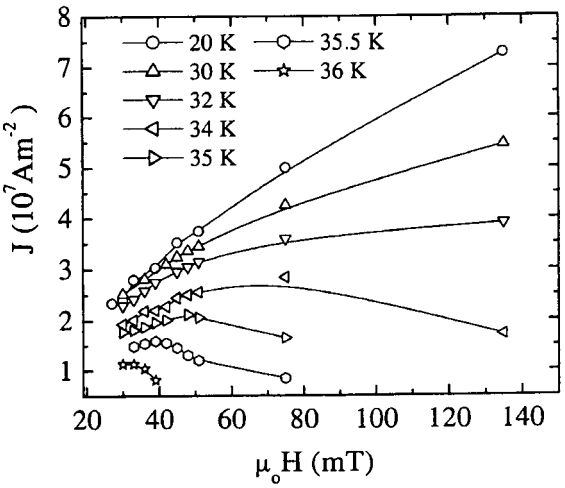

Fig. 5. Sample #2. Local current as a function of the external applied field at different temperatures. The reported data are relative to the maximum values of the current profile along the white dashed line of Figure 2c. Lines are guides for the eye.

again outlined all along the chosen region by the dependence on the field at the different temperatures. The full penetration regime sets up when the curves reach the maximum. Above, the critical current density decreases with the field.

Discussion and conclusions

The results of a MO analysis of good quality MgB_2 bulk-samples are presented. In this paper we show that the samples enter a critical state in a crystal-like fashion. In order to study this critical state, both qualitative and quantitative approaches were used. For the latter, we chose a particularly feature-rich sample. Penetration profiles, current paths and current magnitude in correspondence to these features are shown and are correlated to each other in the critical state framework. The local variation of the maximum supercurrent magnitude with field and temperature in a regime below full penetration, at full penetration and above full penetration regime is calculated.

For type II granular superconductors it is expected that fluxons enter as Josephson vortices through grain boundaries, and that this occurs at field lower than the H_{c1} relative to the grains; Chen *et al.* [21,22], demonstrated that, above a current threshold, a transition from the vortex state to the critical state sets up inside a network of Josephson Junctions (JJs). In that case, the superconductor apparently behaves as a whole. Thus our observations of granularity from one hand, and strong coupling, strong pinning from the other hand, would become consistent if we assume that the microstructural grain-boundary network has a magnetic counterpart in a disordered JJ network, lacing the sample all around large grains [23]. It seems reasonable directing future investigation towards this issue.

We acknowledge the support of INFM (National Institute of Physics of Matter) and of the Italian Space Agency under ARS/99/16 project. The authors wish to thank Dr. E.Bennici for SEM characterisation.

References

1. A.A. Polyanskii, X.Y. Cai, D.M. Feldmann, D.C. Larbalestier, in *Proc. of NATO Advanced Research Workshop (Sozopol, Bulgaria, Sept. 1998)*, edited by I. Nedkov, M. Ausloos, NATO Sciences Series 3: High Technology, Vol. 72 (1999), p. 353.
2. J. Nagamatsu, N. Nakagawa, T. Muranaka, Y. Zenitani, J. Akimitsu, Nature **410**, 63 (2001).
3. D.C. Larbalestier, L.D. Cooley, M.O. Rikel, A.A. Polyanskii, J. Jiang, S. Patnaik, X. Y. Cai., D.M. Feldmann, A. Gurevich, A.A. Squitieri, M.T. Naus, C.B. Eom, E.E. Hellstrom, R.J. Cava, K.A. Regan, N. Rogado, M.A. Hayward, T. He, J.S. Slusky, P. Khalifah, K. Inumaru, M. Haas, Nature **410**, 187 (2001).
4. A.A. Polyanskii, A. Gurevich, J.Y. Jiang, D.C. Larbalestier, S.L. Bud'ko, D.K. Finnemore, G. Lapertot, P.C. Canfield, Supercond. Sci. Technol. **14**, 811 (2001).
5. M. Kambara, N. Hari Babu, E.S. Sadki, J.R. Cooper, H. Minami, D.A. Cardwell, A.M. Campbell, I.H. Inoue, Supercond. Sci. Technol. **14**, L5 (2001).
6. T. Shields, K. Kawano, D. Holdom, J.S. Abell, `http://xxx.lanl.gov/format/cond-mat/0107034`.
7. L. Gozzelino, F. Laviano, D. Botta, A. Chiodoni, R. Gerbaldo, G. Ghigo, E. Mezzetti, G. Giunchi, S. Ceresara, G. Ripamonti, M. Poyer, `http://xxx.lanl.gov/format/cond-mat/0104069`.
8. Edison S.p.A., patent pending.
9. L. Gozzelino, A. Chiodoni, R. Gerbaldo, G. Ghigo, F. Laviano, E. Mezzetti, B. Minetti, R. Fastampa, Inter. J. Mod. Phys. B **14**, 2866 (2000).
10. A. Forkl, H. Kronmüller, Phys. Rev. B **52**, 16130 (1995).
11. P. Brull, D. Kirchgässner, P. Leiderer, Physica C **182**, 339 (1991).
12. L. Dorosinskii, M.V. Indenbom, V.I. Nikitenko, Yu.A. Ossip'yan, A.A. Polyanskii, V.K. Vlasko-Vlasov, Physica C **203**, 149 (1992).
13. Th. Schuster, M. Leghissa, M.R. Koblischka, H. Kuhn, H. Kronmüller, G.G. Saemann-Ischenko, Physica C **203**, 203 (1992).
14. Th. Schuster, M.V. Indenbom, M.R. Koblischka, H. Kuhn, H. Kronmüller, Phys. Rev. B **49**, 3443 (1994).
15. Th. Schuster, H. Kuhn, M.V. Indenbom, Phys. Rev. B **52**, 15621 (1995).
16. Th. Schuster, H. Kuhn, E.H. Brandt, M.V. Indenbom, M. Kläser, G. Müller-Vogt, H.U. Habermeier, H. Kronmüller, A. Forkl, Phys. Rev. B **52**, 10375 (1995).
17. B.J. Roth, J. Appl. Phys. **65**, 361 (1989).
18. Ch. Jooss, R. Warthmann, A. Forkl, H. Kronmüller, Physica C **299**, 215 (1998).
19. E.H. Brandt, M. Indenbom, Phys. Rev. B **48**, 12893 (1993).
20. E.H. Brandt, Phys. Rev. Lett. **74**, 3025 (1995).
21. D.X. Chen, J.J. Moreno, A. Hernando, Phys. Rev. B **53**, 6579 (1996).
22. D.X. Chen, J.J. Moreno, A. Hernando, Phys. Rev. B **56**, 2364 (1997).
23. E. Mezzetti, A. Chiodoni, R. Gerbaldo, G. Ghigo, L. Gozzelino, B. Minetti, C. Camerlingo, C. Giannini, Eur. Phys. J. B **19**, 357 (2001).